Materials Letters: X 3 (2019) 100020

Contents lists available at ScienceDirect

Materials Letters: X

journal homepage: www.elsevier.com/locate/mlblux

Synthesis of Fe_2O_3/biochar nanocomposites by microwave method for magnetic energy-storage concentration cells

Ying Zhang [a], Marina Z. Joel [b], Ying He [c], Daria Weathersby [a], Fengxiang Han [a], Gaurab Rimal [d], Jinke Tang [d], Qilin Dai [a,*]

[a] Department of Chemistry, Physics, and Atmospheric Sciences, Jackson State University, Jackson, MS 39217, USA
[b] Department of Molecular Biophysics and Biochemistry, Yale University, New Haven, CT 06520, USA
[c] Institute of Electronics, Chinese Academy of Science, Beijing 100190, China
[d] Department of Physics & Astronomy, University of Wyoming Laramie, Wyoming 82071, USA

ARTICLE INFO

Article history:
Received 11 April 2019
Received in revised form 25 May 2019
Accepted 30 May 2019
Available online 7 June 2019

Keywords:
Magnetic nanocomposites
Iron oxide nanoparticles
Microwave
Magnetic concentration cells

ABSTRACT

Magnetic nanocomposites have attracted increasing attention due to its widely applications in different areas in recent years. The conventional synthesis of magnetic nanocomposites is usually based on high temperature annealing technique from biomass. In this paper, a microwave method has been developed to prepare iron oxide based magnetic nanocomposites using ferric acetylacetonate ($(Fe(acac)_3$), oleylamine (OAm), oleic acid (OA), and commercial biochar. The reaction is completed in several minutes. Composite structure composed of γ-Fe_2O_3 nanoparticles with the size of 6–17 nm and biochar is confirmed by TEM, SEM EDX element mapping images. The iron oxide size can be controlled by the microwave time and the ligand ratio. Magnetic properties of the magnetic nanocomposites are studied. The application of the prepared magnetic nanocomposites in magnetic concentration cells are tested with different magnetic fields and different biochar to iron oxide ratios. The method developed in this work on magnetic nanocomposite synthesis will not only facilitate the research progress of magnetic nanocomposite synthesis but also provide an alternative technique to be used in magnetic concentration cells.

1. Introduction

Biochar is carbon rich residue produced through pyrolysis of biomass in the absence of oxygen, and, biochar could help CO_2 removal and mitigate climate change [1–6]. With porous properties, biochar has attracted increasing attention with many applicants, such as pollutant removal, cathode materials in battery and soil fertility [7–12]. Magnetic modification is one of most hot topics in biochar research, which combines the magnetic properties and high surface area of biochar, leading to novel applications [13,14]. The synthesis of magnetic nanocomposites is usually achieved by decomposition of iron salt into oxide in presence of biomass material during pyrolysis [15]. Iron oxide nanoparticles are synthesized in the presence of biochar. However, this process requires high temperature annealing, long reaction time, and the production of iron oxide nanoparticles cannot be controlled due to the nature of inorganic iron salt decomposition reaction. New magnetic nanocomposite synthesis is very necessary for magnetic nanocomposite research. Microwave is one of the novel technologies for magnetic nanocomposite synthesis with the advantage of short time consuming and high production yield. Yap et al. reported the synthesis of magnetic nanocomposites by pyrolysis of mixture of biomass (coconut shells) and $FeCl_3{\cdot}6H_2O$ in microwave muffle system oven [16]. Zubrik et al. also reported the pyrolysis of the mixture of biomass (wheat straw) and ferrofluid, and successfully produced the magnetic nanocomposites with various Fe-bearing phase with size from several to 100 nm [17]. However, it is hard to control the magnetic properties of the magnetic nanocomposites by their methods, and the size distribution of their magnetic nanoparticles is very large, which influence the application of magnetic nanocomposites.

In addition, magnetic electrolyte concentration cells based on magnetic nanoparticles have been reported for energy storage, producing voltage and current output controlled by a large concentration gradient realized with external magnetic field switching [18]. Magnetic nanoparticles passivated by surface ligands, such as citric acid ligands, are used as electrolytes in magnetic concentration cells. Under external magnetic field, magnetic nanoparticles, as ligand carriers, coated by citric acid ligands will be attracted, and a large citric acid concentration gradient will be created and, which can induce current/voltage generation.

* Corresponding author.
E-mail address: qilin.dai@jsums.edu (Q. Dai).

https://doi.org/10.1016/j.mlblux.2019.100020
2590-1508/

The magnetic concentration cells are recyclable, low-cost, environmental friendly and fast responsible compared with the conventional concentration cells [18]. Magnetic concentration cells performance is dictated by the magnetic properties and surface area of the ligand carriers. The magnetic nanocomposites with excellent magnetic properties and large surface area is promising for magnetic concentration cell application.

In this work, a novel method is developed to prepare magnetic nanocomposites by microwave method, with $Fe(acac)_3$, oleylamine (OAm), oleic acid (OA) and biochar. This method takes several mins and does not need high temperature annealing process. The nanoparticle growth can be controlled by microwave time and OAm to OA ratio. The iron oxide nanoparticles grow on biochar structure forming iron oxide/biochar composite. By this method, the magnetic nanoparticles can be controlled in terms of size, and structure, which may tune the magnetic properties of the magnetic nanocomposites. Meanwhile, magnetic nanocomposites with large surface area modified with citric acid ligands are used as electrolytes in magnetic concentration cells. Voltage output is controlled by different external magnetic fields and magnetic nanocomposites with different iron oxide nanoparticles.

2. Method

2.1. Experimental

Fe_2O_3 based magnetic nanocomposites were prepared by microwave method. In a typical synthesis, a mixture solution of OAm from TCI, OA from Alfa Aesar with certain ratio was prepared in a beaker. Then, $Fe(acac)_3$ from Alfa Aesar and Biochar from Biochar Now (gridded and sieved to 200 mesh) were added to the above mixture solution. Then, the mixture was heated by microwave oven (Hamilton Beach) for different time. The solution was cooled down to room temperature, and iron oxide nanoparticles or magnetic nanocomposites were precipitated by adding ethanol. The product was washed five times by toluene and methanol and then dried under vacuum. Table 1 shows the experimental parameters of the reaction and the sample information.

2.2. Measurements

Powder X-ray diffraction (XRD) data were recorded by Rigaku MiniFlex 600 X-ray Diffractometer. The magnetic hysteresis (M-H) loop measurements of the magnetic nanocomposites powder samples were carried out on a Physical Properties Measurement System (PPMS) (Quantum Design). Transmission electron microscope (TEM) images were obtained by a JEM-1011 Transmission Electron Microscope (JEOL) and FEI Tecnai G2 F20 Transmission Electron Microscope. For TEM test of magnetic nanocomposites, samples are re-gridded and re-suspended in water, aging for a while, then the supernatant is used to prepare TEM measurements Energy Dispersive Spectroscopy (EDS) results were collected on Scanning Electron Microscopy (TESCAN LYRA3).

2.3. Concentration cell test

Concentration cell container was made by attaching copper sheets (0.4 mm thickness) as electrodes by glue on the two ends of a plastic container (3.4 cm × 1.0 cm), the distance between these two electrodes is 1.0 cm. The Fe_2O_3/biochar nanocomposites was soaked in citric acid ethnol solution for 10 min. Then filled the container with citric acid ethnol solution and Fe_2O_3/biochar nanocomposites. Voltage signals were measured by a CHI 604E electrochemical workstation. Magnetic fields provided by a magnet (from Master Magnetics) was used to switch directions every 20 s.

3. Results and discussion

Fig. 1a shows the reaction schematic diagram used in this work. Iron oxide nanoparticles will be produced during microwave using OAm, OA and $Fe(acac)_3$. It was reported that OAm and OA can be used to control the metal oxide nanoparticle growth in terms of size, structure, and morphology. It is believed that OAm could play as the reductant as well as the weak capping agent, and the OA could play as the capping agent [19–21]. Microwave is a very promising technique to synthesize nanoparticles due to shorter reaction time and high reproducibility [22]. Therefore, microwave technique was used here as a fast route to prepare magnetic nanocomposites by iron oxide in the presence of biochar. Iron oxide nanoparticles will grow on biochar structure to form iron oxide/biochar composite, which provide a strategy to control the properties of magnetic nanoparticles on magnetic nanocomposites. Fig. 1b–d shows TEM images of S1, S2 and S3 respectively. Monodispersed spherical nanoparticles can be observed in the Figure. The insets exhibit the corresponding size distribution analyzed by Nanomeasure software. The average sizes of S1, S2 and S3 are 6 nm, 7 nm and 9 nm respectively, which can be understood by the increased ratio of Fe to organic ligands. According to Patel's suggestion, higher ratio of Fe to ligands leads to higher concentration of Fe ions in the microwave precursor, which will provide more Fe^{3+} ions to form iron oxide nanoparticles [23]. Different OAm to OA ratios and microwave time are also used to control iron oxide nanoparticle growth. Fig. 1e and f presents the TEM images and size distribution of S4 and S5, which was prepared with different microwave and different ratio of OAm to OA. The mean size of S4 is 12 nm, which is larger than that of S2 (7 nm) indicating iron oxide nanoparticles grow larger as the microwave time increases. It is reported that different capping capabilities of OAm and OA can cause selective facet passivation during nanoparticle growth, which can result in different nanoparticle morphology [19–21]. However, it can be seen that the nanoparticle shape does not change that much as the ratio of OAm to OA varies from our results, the average size of S5 is also 12 nm. The increased particle size compared to S2 (7 nm) can be attributed to absence of OA in the reaction. OAm has weaker capping capability compared to OA [19–21], which leads to larger nanoparticles as only OAm used to passivate the nanoparticles.

Table 1
Sample informations.

Sample name	Fe (g)	OAm (mmol)	OA (mmol)	Biochar (g)	Microwave time (min)	Mean size (nm)
S1	0.5	11.5	12.2	0	10	6
S2	1	11.5	12.2	0	10	7
S3	2	11.5	12.2	0	10	9
S4	1	11.5	12.2	0	30	12
S5	1	23.0	0	0	10	12
S2-B	1	11.5	12.2	1	10	7
S6-B	1	11.5	12.2	0.5	10	17
S7-B	1	11.5	12.2	0.25	10	10

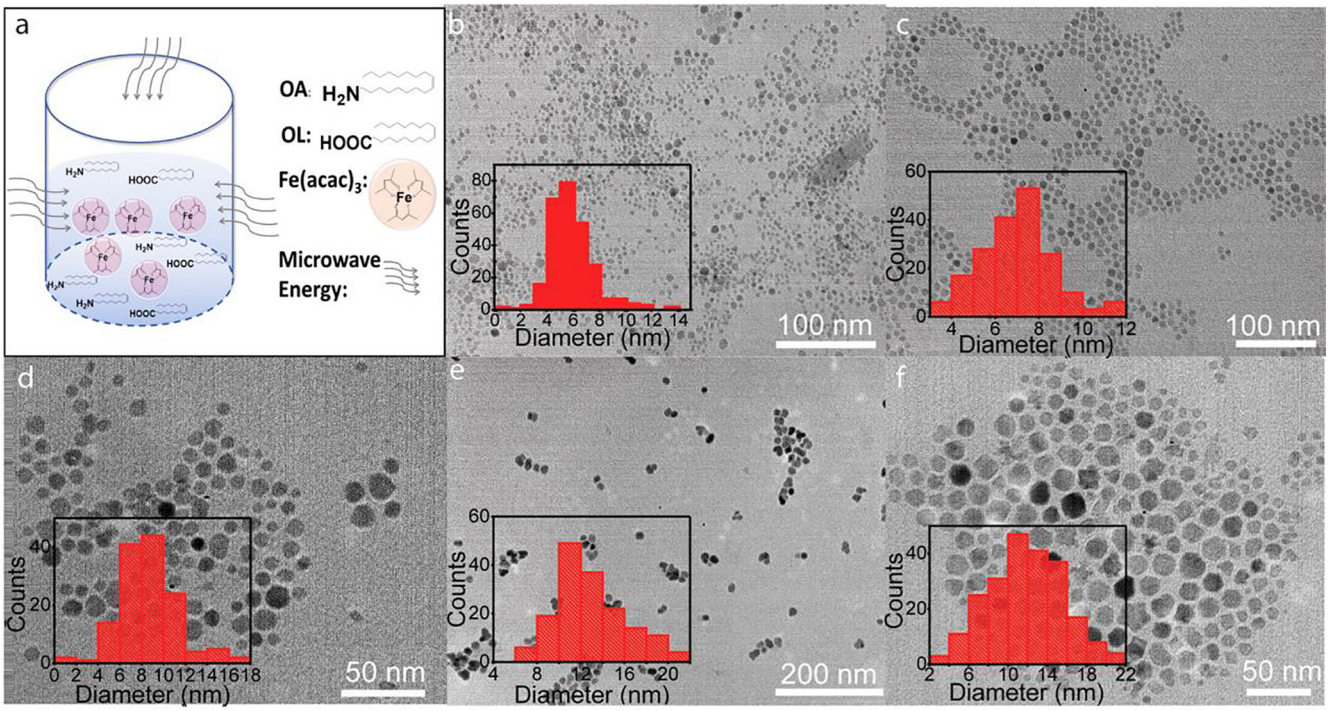

Fig. 1. (a) The microwave synthesis mechanism of iron oxide by Fe(acac)$_3$, OAm, and OA. (b)–(f) show the TEM images S1, S2, S3, S4, and S5 respectively. The insets of b, c, d, e and f exhibit the corresponding size distribution.

Magnetic nanocomposites were obtained by adding the biochar into the iron oxide microwave precursor. Fig. 2 shows the results of iron oxide/biochar. In Fig. 2a, typical porous structure can be observed indicating the large surface area of the biochar. TEM images of magnetic nanocomposite S2-B are shown in Fig. 2b and c. Irregular shape biochar is shown in the TEM images, and porous structure is missing. This is attributed to the broken biochar. Typically, two types of structure can be observed by TEM study. Block structures and fiber structures are exhibited in Fig. 2b and c respectively. Composite structure is confirmed by the TEM images. Smaller nanoparticles and large transparent structures can be observed. The smaller nanoparticles are iron oxide nanoparticles, and the large structure is biochar. Iron oxide nanoparticles are attached onto biochar, indicating that the composite structure were successfully formed. There are still some free iron oxide nanoparticles in the TEM image which does not affect the overall magnetic nanocomposite properties significantly. Different ratios of iron oxide to biochar are designed to control the magnetic properties of the obtained magnetic nanocomposites and the iron oxide nanoparticle growth. Fig. 2d and e shows the TEM images of S6-B and S7-B iron oxide/biochar with less biochar component compared to Fig. 2b and c. The size distribution information is exhibited in the inset of the Figures. The average sizes of S6-B and S7-B are 17 nm and 10 nm respectively. For S2, S7-B and S6 B, the average size of the iron oxide nanoparticles increases from 7 nm to 17 nm as the biochar component increases from 0 g to 0.5 g. Then as the biochar component further increases to 1 g (S2-B), the average size decreases. Two mechanisms compete with each other as the biochar component increases. First, iron oxide nuclei will get close to each other as biochar is added to the solution due to the same volume utilized in all the reactions, leading to increased nanoparticle size. Second, more biochar in the microwave precursor absorbs more microwave energy, resulting in less energy applied to Fe(acac)$_3$ precursor and smaller nanoparticles. The two above mechanisms explain the trend of nanoparticle size influenced by the amount of biochar. The phase structure of the biochar and the prepared magnetic nanocomposites are studied by powder XRD technique. Fig. 2f shows the XRD diffraction patters of sample S2-B, S7-B and bare biochar. The diffraction peaks of biochar at 20.9°, 21.26°, 26.66° and 27.54° are from quartz, sylvite and calcite according to the literature [24], indicating that these inorganic phases are involved in the biochar during production. S7-B shows clear diffraction peaks at 30.3°, 35.7°, 43.3°, 53.8°, 57.4°, and 63.0°, which are assigned to (2,0,6), (1,1,9), (0,0,12), (2,2,12), (1,1,15), (4,4,12) of γ-Fe_2O_3 (JCPDS25-1402) [25,26]. S2-B exhibits one peak from γ-Fe_2O_3 at 35.7° only, which is attributed to the limited amount of Fe(acac)$_3$ starting materials in the S2-B synthesis process compared to that of S7-B. In S2-B and S7-B samples, the diffraction features of biochar are also observed, and no additional peaks formed. The above discussion suggests that our microwave process can produce pure γ-Fe_2O_3 and does not destroy biochar structure, leading to magnetic nanocomposite synthesis. To study the stability of iron oxide/biochar composition, the magnetic nanocomposites have been suspended in ethanol with strong stirring for 10 min. The TEM pictures from before and after stirring show no significant difference, which indicates that the iron oxide nanoparticles are firmly attached onto the biochar, and cannot be easily removed (Fig. S1). To confirm the composite structure, SEM EDX element mapping data are acquired and shown in Fig. 2g–i. Fig. 2h and i show the carbon and iron element mapping images respectively. It can be seen that the carbon and iron element images are consistent with the raw SEM image in Fig. 2g, indicating the homogeneous distribution of iron oxide in the biochar structure and the successful composite structure.

The iron oxide-biochar nanocomposites were synthesized by microwave assisted thermal decomposition of Fe(acac)$_3$ in the mixture of OAm and OA in present of biochar, as shown in Fig. 3. It is reported that OA plays as the capping agent, while OAm plays as both the reducing and capping agents as the reaction is in the absence of oxygen [27]. Sun et al. prepared FeO nanoparticles by the decomposition of Fe(aca)$_3$ in the presence of OAm and OA under inert gas Ar protection [28]. However, in this work, reducing

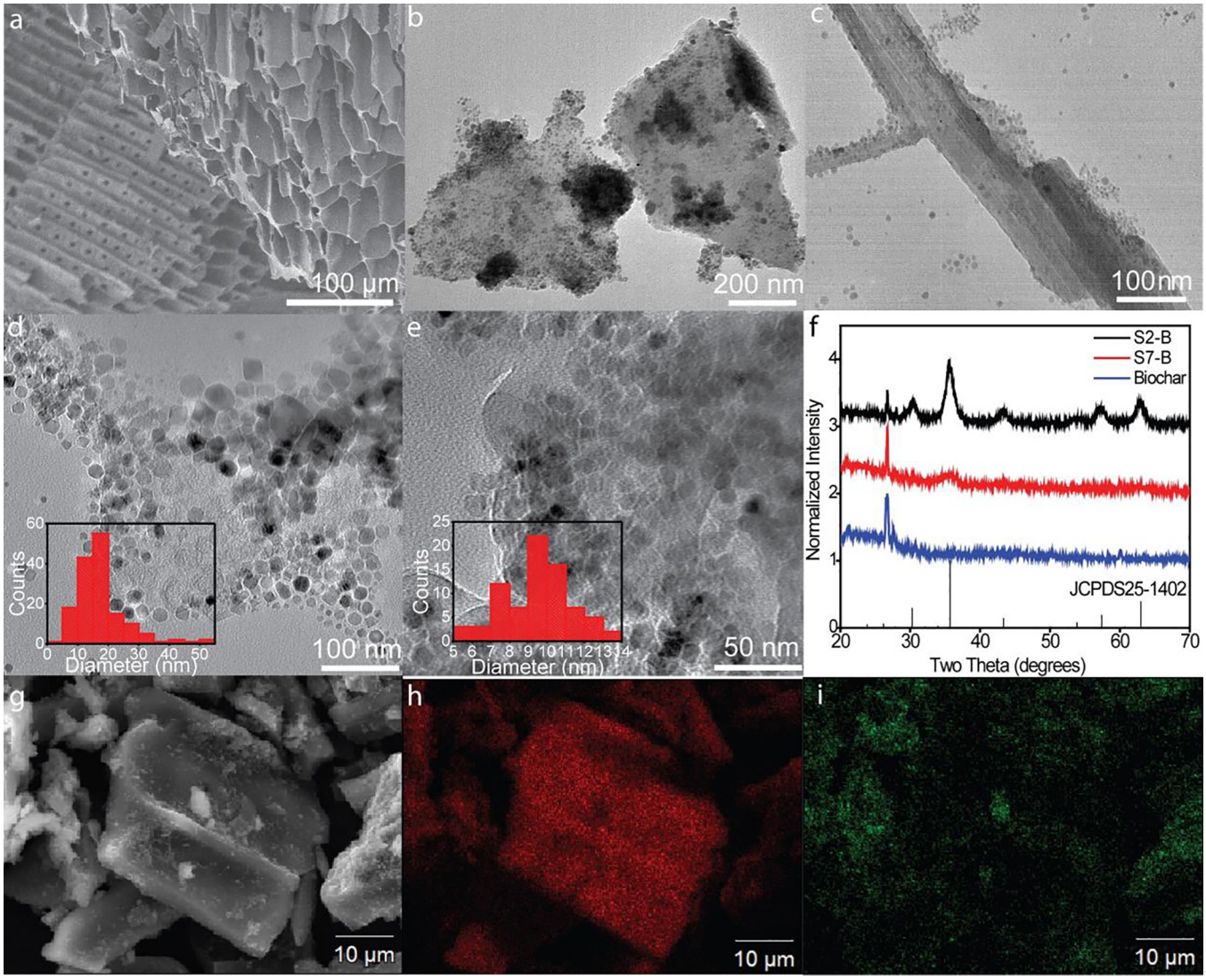

Fig. 2. (a) SEM image of biochar used in this work. (b) and (c) show TEM images of different structures of S2-B magnetic nanocomposites composed of iron oxide and biochar. (d) Shows the TEM image of sample S6-B and corresponding size distribution. (e) Shows TEM image of sample S7-B and corresponding size distribution. f shows the XRD diffraction patterns of S2-B, S7-B and biochar. (g)–(i) Show the SEM EDX element mapping images. (g) is SEM image. (h) is carbon element mapping image. (i) is iron element mapping image.

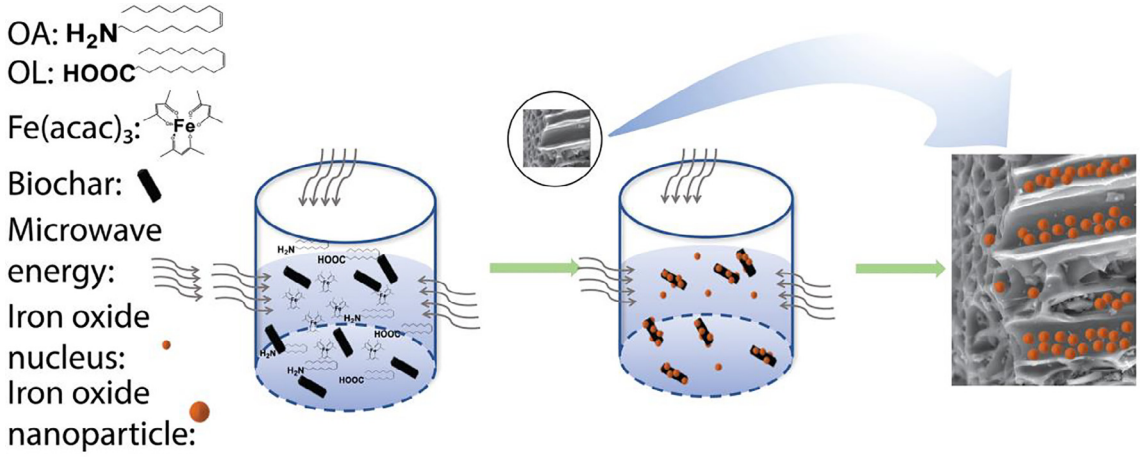

Fig. 3. Magnetic nanocomposites growth mechanism.

effect of OAm is not observed. It is possible that oxygen in the air decreases the reducing effect of OAm, leading to the production of Fe_2O_3 nanoparticles. With energy from microwave, the mixture was heated up to high temperature in several seconds. γ-Fe_2O_3 seeds were formed in the biochar structure in the solution at the first stage of the reaction. Then large nanoparticles were produced by consuming the seeds in the biochar framework, leading to nanocomposite structure. Finally, γ-Fe_2O_3 nanoparticle growth was terminated by the surface passivants including OAm and OA, leading to the nanocomposite production in biochar structure. It is reported that the sizes and morphology of nanoparticles can be controlled by the organic passivants, typically OAm and OA, due to the selective facet capping capabilities [19,29,30]. However, in this work, only sizes of the nanoparticles can be tuned by the reaction parameters including the ratios of ligands and microwave time. Usually, it is hard to prepare magnetic nanoparticles with different shapes. This can be explained by the relative week capping capabilities of the ligands compared to the crystal structure anisotropy.

The magnetic nanocomposite with large surface area due to porous structure from biochar and magnetic properties from iron oxide enable its application on magnetic concentration cells, where citric acid ligands are adsorbed on magnetic nanocomposites to generate large concentration gradient of the ligands by external magnetic field. Fig. 4a shows room temperature magnetic hysteresis loop of the prepared magnetic nanocomposite S2-B. The inset shows a photograph of the prepared magnetic nanocomposites in an ethanol solution attracted by an external magnetic field. From the hysteresis loop, it can be observed that the coercivity and saturation magnetic moment are zero and 0.0032 emu/g respectively. The zero coercivity suggests superparamagnetic behavior of the γ-Fe_2O_3 nanoparticles and is consistent with the published results [31,32]. The small saturation magnetic moment is attributed to the mass of biochar in magnetic nanocomposites, which does not contribute to the magnetic moment. Fig. 4b shows the S2-B magnetic concentration cell device performance operated under different magnetic fields. The voltage output is about 0.005 V as the external field is 600 Oe. The voltage output increases to 0.006 V as the external field increases to 1300 Oe. ~0.01 V voltage output is exhibited as the external field increases to 4600 Oe. As large magnetic field is used to the magnetic concentration cell, the maximum voltage output increases which can be ascribed to the strong attraction of magnetic nanocomposites, which, resulting in increased concentration gradient and large voltage output. Fig. 4c shows the voltage ramping time of the S2-B device performance under different external magnetic fields. As 200 Oe is applied to the device, no voltage output can be detected due to the external field is too small to move the magnetic nanocomposites. The ramping time is determined by the diffusion speed of magnetic nanocomposites under the external magnetic field. A small magnetic field causes a slow diffusion of magnetic nanocomposites, leading to a longer ramping time compared to that of the large magnetic field. Therefore, shorter ramping time is observed for the large field 4600 Oe in comparison with small field 600 Oe. Fig. 4d shows the performance of the devices based on S2-B and S7-B measured by the same external magnetic field 4600 Oe. Small voltage output of 0.025 V is observed for the S7-B based device compared to 0.01 V for that of S2-B based device. This can be explained by the relative large amount of biochar in S2-B sample. Yan et al. studied the concentration cells with Fe_3O_4 as carrier, and got the hight output voltage about 0.5 V [33]. We studied the concentration cell with cobalt ferrite (CFO) nanocrystals as carriers, and reported the voltage output of 60 mV for CFO nanocrystal with size of 10 nm, and voltage output decreased to 20 mV for CFO nanocrystal with size of 110 nm. This decreased performance is attributed to reduced surface area [34]. We used $NiFe_2O_4$

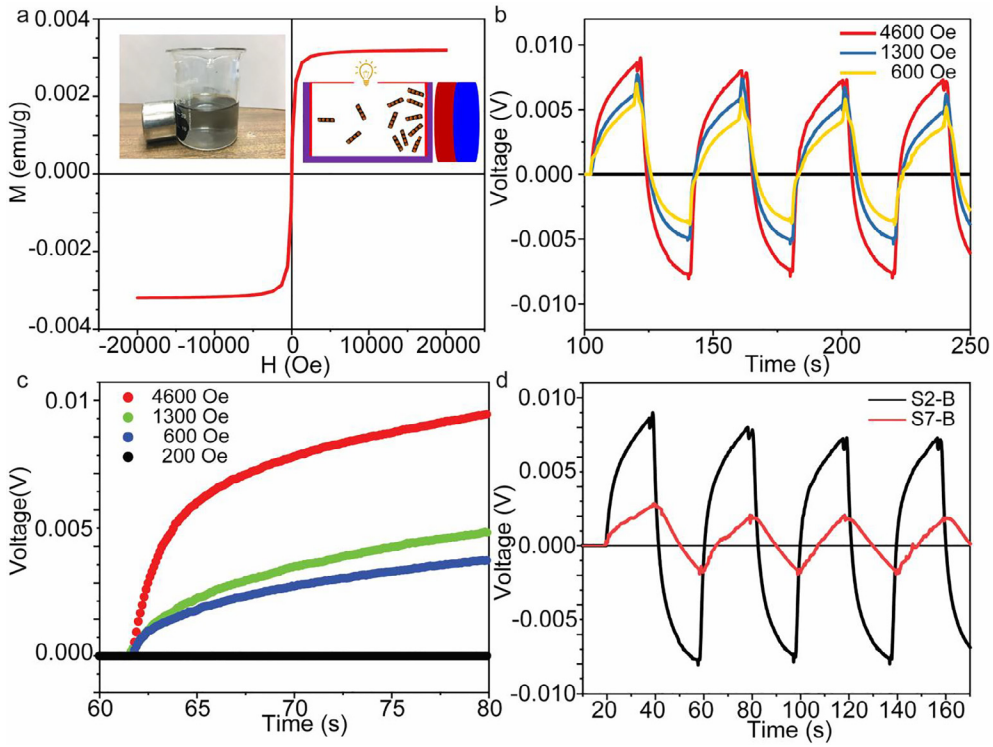

Fig. 4. (a) Magnetic hysteresis loop of magnetic nanocomposites S2-B. The left inset shows a photograph image of a magnetic nanocomposites in an aqueous solution attracted by external magnetic field. The right inset shows the schematic of a magnetic concentration cell. (b) Magnetic concentration cell voltage output of device based on S2-B under different magnetic fields. (c) Voltage ramping time of the S2-B device switched by different magnetic fields. (d) Magnetic concentration cell voltage output of the devices based on S2-B and S7-B.

nanoparticle as carrier for concentration cells, and obtained the output voltage of 0.04 V with nanoparticle size of 30 nm, and 0.02 V with size of 200 nm [35]. In this work, our concentration cells with Fe_2O_3/biochar nanocomposites as carrier showed comparable results compared to our previous results. Citric acid ligands can be adsorbed by iron oxide nanoparticles and biochar. The low voltage output is attributed to the low concentration gradient caused by some free biochar or the inhomogeneous distribution of iron oxide nanoparticles in biochar matrix.

4. Conclusion

In this work, a microwave method has been developed to synthesize magnetic nanocomposites via $Fe(acac)_3$ and biochar in organic ligands OAm and OA. Composite structure of iron oxide/biochar is obtained in several minutes due to the fast reaction by microwave technique. The size of iron oxide nanoparticles (6–17 nm) can be controlled by the reaction parameters including microwave time and organic ligand ratio. By this method, high temperature annealing process is avoided, and this developed method provide a platform to control the nanoparticle growth compared to the traditional method for preparing magnetic nanocomposites. The applications of the prepared magnetic nanocomposites in magnetic concentration cells has been studied. ~0.01 V voltage output is obtained by the device based on sample S7-B. Further studies are needed to optimize the device performance.

Declaration of Competing Interest

There are no conflicts of interest related to this paper for the authors.

Acknowledgements

This work was supported by National Science Foundation (NSF) award 1632899 and 1332444, and University of Wyoming School of Energy Resources via the Carbon Engineering Initiative. The XRD used in this work was supported by the U.S. Army Engineer Research and Development Center (W912HZ-16-2-0021).

Appendix A. Supplementary data

Supplementary data to this article can be found online at https://doi.org/10.1016/j.mlblux.2019.100020.

References

[1] J. Lehmann, S. Joseph, Biochar for Environmental Management: Science, Technology and Implementation, Routledge, 2015.
[2] D. Woolf, J.E. Amonette, F.A. Street-Perrott, J. Lehmann, S. Joseph, Sustainable biochar to mitigate global climate change, Nat. Commun. 1 (2010) 56.
[3] L. Van Zwieten, S. Kimber, S. Morris, K. Chan, A. Downie, J. Rust, S. Joseph, A. Cowie, Effects of biochar from slow pyrolysis of papermill waste on agronomic performance and soil fertility, Plant Soil 327 (1–2) (2010) 235–246.
[4] M. Ahmad, A.U. Rajapaksha, J.E. Lim, M. Zhang, N. Bolan, D. Mohan, M. Vithanage, S.S. Lee, Y.S. Ok, Biochar as a sorbent for contaminant management in soil and water: a review, Chemosphere 99 (2014) 19–33.
[5] P. Sujana, The application of biochar to screen printing liquid waste polluted land, its effect in soil, mustard greens to heavy metals (Fe, Cr), Res. J. Textile Apparel (2018).
[6] K.A. Sarpong, A. Salazar, A. Ortega, K. Telles, K. Djaman, M.K. O'Neill, D.J. Valles-Rosales, C.E. Brewer, Pyrolysis of wood excelsior residues for biochar and renewable energy production, in: 2018 ASABE Annual International Meeting, American Society of Agricultural and Biological Engineers, 2018, p. 1.
[7] J. Yang, T. Ma, X. Li, J. Tu, Z. Dang, C. Yang, Removal of heavy metals and metalloids by amino-modified biochar supporting nanoscale zero-valent iron, J. Environ. Qual. (2018).
[8] S. Huang, J. Bao, M. Shan, H. Qin, H. Wang, X. Yu, J. Chen, Q. Xu, Dynamic changes of polychlorinated biphenyls (PCBs) degradation and adsorption to biochar as affected by soil organic carbon content, Chemosphere (2018).
[9] H.W. Lee, Y.-M. Kim, S. Kim, C. Ryu, S.H. Park, Y.-K. Park, Review of the use of activated biochar for energy and environmental applications, Carbon Lett. 26 (1) (2018) 1–10.
[10] Z.-H. Chen, X.-L. Du, J.-B. He, F. Li, Y. Wang, Y.-L. Li, B. Li, S. Xin, Porous coconut shell carbon offering high retention and deep lithiation of sulfur for lithium–sulfur batteries, ACS Appl. Mater. Interfaces 9 (39) (2017) 33855–33862.
[11] A.B. Cobb, G.W. Wilson, C.L. Goad, M.A. Grusak, Influence of alternative soil amendments on mycorrhizal fungi and cowpea production, Heliyon 4 (7) (2018).
[12] A. El-Naggar, S.S. Lee, Y.M. Awad, X. Yang, C. Ryu, M. Rizwan, J. Rinklebe, D.C. Tsang, Y.S. Ok, Influence of soil properties and feedstocks on biochar potential for carbon mineralization and improvement of infertile soils, Geoderma 332 (2018) 100–108.
[13] C.-D. Dong, C.-W. Chen, C.-M. Hung, Persulfate activation with rice husk-based magnetic biochar for degrading PAEs in marine sediments, Environ. Sci. Pollut. Res. (2018) 1–10.
[14] S. Pourhosseini, O. Norouzi, P. Salimi, H.R. Naderi, Synthesis of a novel interconnected 3D pore network algal biochar constituting iron nanoparticles derived from a harmful marine biomass as high-performance asymmetric supercapacitor electrodes, ACS Sustainable Chem. Eng. 6 (4) (2018) 4746–4758.
[15] B. Chen, Z. Chen, S. Lv, A novel magnetic biochar efficiently sorbs organic pollutants and phosphate, Bioresour. Technol. 102 (2) (2011) 716–723.
[16] M. Yap, N. Mubarak, J. Sahu, E. Abdullah, Microwave induced synthesis of magnetic biochar from agricultural biomass for removal of lead and cadmium from wastewater, J. Ind. Eng. Chem. 45 (2017) 287–295.
[17] A. Zubrik, M. Matik, M. Lovás, K. Štefušová, Z. Danková, S. Hredzák, M. Václavíková, F. Bendek, J. Briančin, L. Machala, One-step microwave synthesis of magnetic biochars with sorption properties, Carbon Lett. 26 (1) (2018) 31–42.
[18] Q. Dai, K. Patel, G. Donatelli, S. Ren, Magnetic cobalt ferrite nanocrystals for an energy storage concentration cell, Angew. Chem. Int. Ed. 55 (35) (2016) 10439–10443.
[19] Q. Dai, J. Tang, The optical and magnetic properties of CoO and Co nanocrystals prepared by a facile technique, Nanoscale 5 (16) (2013) 7512–7519.
[20] Q. Dai, J. Tang, Magnetic properties of CoO nanocrystals prepared with a controlled reaction atmosphere, RSC Adv. 3 (24) (2013) 9228–9233.
[21] V. Abdelsayed, A. Panda, G. Glaspell, M. El-Shall, R. Nagarajan, T. Hatton, Nanoparticles: synthesis, stabilization, passivation, and functionalization, ACS Symp. Ser. (2008) 225–247.
[22] Q. Dai, M.E. Foley, C.J. Breshike, A. Lita, G.F. Strouse, Ligand-passivated Eu: Y_2O_3 nanocrystals as a phosphor for white light emitting diodes, J. Am. Chem. Soc. 133 (39) (2011) 15475–15486.
[23] H.E. Patel, S.K. Das, T. Sundararajan, A. Sreekumaran Nair, B. George, T. Pradeep, Thermal conductivities of naked and monolayer protected metal nanoparticle based nanofluids: manifestation of anomalous enhancement and chemical effects, Appl. Phys. Lett. 83 (14) (2003) 2931–2933.
[24] M. Lawrinenko, D.A. Laird, Anion exchange capacity of biochar, Green Chem. 17 (9) (2015) 4628–4636.
[25] J. Huang, S. Yang, Y. Xu, X. Zhou, X. Jiang, N. Shi, D. Cao, J. Yin, G. Wang, Fe_2O_3 sheets grown on nickel foam as electrode material for electrochemical capacitors, J. Electroanal. Chem. 713 (2014) 98–102.
[26] S.-Z. Guo, Y. Li, J.-S. Jiang, H.-Q. Xie, Nanofluids containing γ-Fe_2O_3 nanoparticles and their heat transfer enhancements, Nanoscale Res. Lett. 5 (7) (2010) 1222.
[27] Z. Xu, C. Shen, Y. Hou, H. Gao, S. Sun, Oleylamine as both reducing agent and stabilizer in a facile synthesis of magnetite nanoparticles, Chem. Mater. 21 (9) (2009) 1778–1780.
[28] Y. Hou, Z. Xu, S. Sun, Controlled synthesis and chemical conversions of FeO nanoparticles, Angew. Chem. 119 (33) (2007) 6445–6448.
[29] V. Abdelsayed, A.B. Panda, G.P. Glaspell, M.S. El Shall, Synthesis, passivation, and stabilization of nanoparticles, nanorods, and nanowires by microwave irradiation, nanoparticles: synthesis, stabilization, passivation, and functionalization, Am. Chem. Soc. (2008) 225–247.
[30] Z.-J. Li, E. Hofman, A.H. Davis, M.M. Maye, W. Zheng, General strategy for the growth of CsPbX3 (X = Cl, Br, I) perovskite nanosheets from the assembly of nanorods, Chem. Mater. 30 (11) (2018) 3854–3860.
[31] M.d.P. Morales, S. Veintemillas-Verdaguer, M. Montero, C. Serna, A. Roig, L. Casas, B. Martinez, F. Sandiumenge, Surface and internal spin canting in γ-Fe_2O_3 nanoparticles, Chem. Mater. 11 (11) (1999) 3058–3064.
[32] W. Zheng, G.F. Strouse, Involvement of carriers in the size-dependent magnetic exchange for Mn: CdSe quantum dots, J. Am. Chem. Soc. 133 (19) (2011) 7482–7489.
[33] Y. Yan, J.V. Timonen, B.A. Grzybowski, A long-lasting concentration cell based on a magnetic electrolyte, Nat. Nanotechnol. 9 (11) (2014) 901.
[34] Q. Dai, K. Patel, G. Donatelli, S. Ren, Magnetic cobalt ferrite nanocrystals for an energy storage concentration cell, Angew. Chem. 128 (35) (2016) 10595–10599.
[35] Y. Zhang, G. Rimal, J. Tang, Q. Dai, Synthesis of $NiFe_2O_4$ nanoparticles for energy and environment applications, Mater. Res. Express 5 (2) (2018) 025023.